

Refractive-index and element-spacing effects on the spectral behavior of infrared frequency-selective surfaces

Irina Puscasu, David Spencer, and Glenn D. Boreman

Transmission and reflection characteristics of inductive-mesh frequency-selective surfaces were measured in the 4–12- μm range. Specific issues investigated include the effect of interelement spacing on the location and width of the resonance and the influence of superstrate and substrate refractive indices on the spectral response of the structure. © 2000 Optical Society of America

OCIS codes: 260.3060.

1. Introduction

A periodic array consisting of conducting-patch or aperture elements^{1–3} is known as a frequency-selective surface (FSS). Depending on the details of the element configuration, the FSS can be designed to exhibit high transmittance or high reflectance at specific wavelengths. Several element geometries have been proposed, including crossed dipoles,^{4,5} Jerusalem crosses,^{6,7} tripoles,⁸ and loops.^{9,10} Most of the reported results have been in the millimeter-wave and far-infrared (IR) region. Bandpass array filters for the 3–12- cm^{-1} (0.83–3-mm) band were reported by Timusk and Richards.¹¹ Low-pass filtering in submillimeter astronomy with capacitive square grids was proposed by Whitcomb and Keene.¹² Tomaselli *et al.*¹³ investigated arrays of cross-shaped elements for far-IR bandpass filters for the 30–80- cm^{-1} band. With continuing advancements in lithography, smaller element dimensions have been achieved, allowing for the fabrication of FSS's with response in the IR portion of the spectrum. Results have been reported for resonant arrays of crosses at 7–9 μm ,¹⁴ 6.5 μm ,¹⁵ and 1.5 μm .¹⁶

In this paper we analyze dipole-patch IR FSS's with resonant responses at wavelengths between 4 and 14 μm . Our investigation centers on two spe-

cific issues: (i) the effect of interelement spacing on the location and width of the resonance and (ii) the influence of superstrate and substrate refractive indices on the resonance wavelength.

2. Fabrication

The substrates for our FSS's were *n*-doped Si wafers of 5- Ω cm resistivity and 380- μm thickness. Some arrays investigated were fabricated directly on top of the Si substrate, and some were deposited on top of a thermally grown, 0.25- μm layer of SiO_2 . A two-layer PMMA/P(MMA-MAA) copolymer resist was used [PMMA is poly(methyl methacrylate)], exposed by a focused electron beam (*e*-beam) from a Cambridge Instruments EBMF-2 pattern generator. The optimum dose was $\approx 480 \mu\text{C}/\text{cm}^2$. The resist was developed in a 1:3 solution of methyl isobutyl ketone and isopropanol. A 30-nm film of aluminum was then deposited by *e*-beam evaporation. A tape-assisted lift-off procedure was used to remove the unexposed resist, followed by an ultrasound-assisted agitation in methylene chloride. An additional step was performed for some of the arrays studied: deposition of a 1- μm overcoat layer of rf-sputtered Si on top of the metallic patches. The along-arm length of the patches L_x and the spacing between elements $D_x = D_y$ were varied in our study (Table 1). In each case, the cross-arm dimension of the patches $L_y \approx 0.13 \mu\text{m}$ and the overall array dimensions were 5 mm \times 5 mm. We also varied the configuration involving the media above and below the FSS and the coupling between the patches (Table 1).

3. Spectral Measurement Procedure

The spectral reflection and transmission of our IR FSS's were measured at normal incidence over the 4–14- μm band with a Perkin-Elmer 1710 IR Fourier

I. Puscasu and G. D. Boreman (boreman@creol.ucf.edu) are with the Center for Research and Education in Optics and Lasers/School of Optics, University of Central Florida, Orlando, Florida 32816-2700. D. Spencer is with the Cornell Nanofabrication Facility, Cornell University, Ithaca, New York 14853-5403.

Received 26 October 1999; revised manuscript received 17 December 1999.

0003-6935/00/101570-05\$15.00/0

© 2000 Optical Society of America

Table 1. Geometrical Dimensions of the Arrays Studied

	Name ^a	Physical Length L_x (μm)	Edge-to-Edge spacing $D_x = D_x$ (μm)
Coupled dipole array on SiO ₂ -Si substrate	(air-SiO ₂ , coupled, 1.6)	1.6	1.32
Coupled dipole array on Si substrate	(air-Si, coupled, 0.8)	0.8	1
	(air-Si, coupled, 1.6)	1.6	1.32
	(air-Si, coupled, 2)	2	1.7
Isolated dipole array on Si substrate	(air-Si, coupled, 0.8)	0.8	1
	(air-Si, coupled, 1.7)	1.7	1
Coupled dipole Si-array-Si	(Si-Si, coupled, 0.8)	0.8	1
	(Si-Si, coupled, 1.6)	1.6	1.32
	(Si-Si, coupled, 2)	2	1.7

^aSubstrate configuration, array configuration, dipole length L_x (μm).

transform spectrometer at a spectral resolution of 4 cm^{-1} .

Figures 1(a) and 1(b) show typical spectral transmittance and reflectance data, respectively, for an IR FSS, along with the spectral characteristics of the substrate alone. It can be seen from these data that

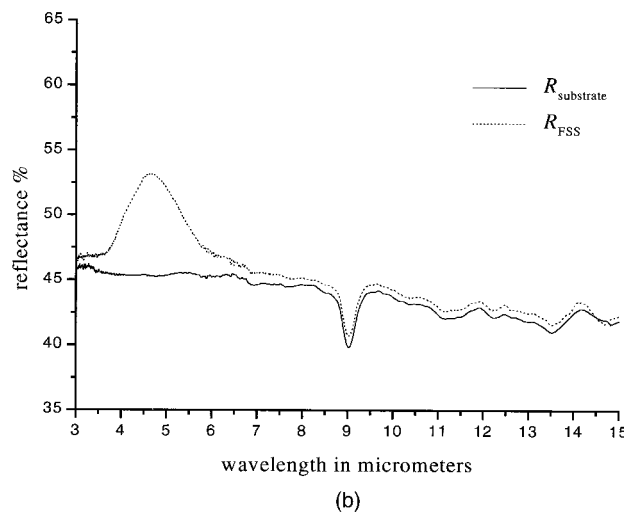
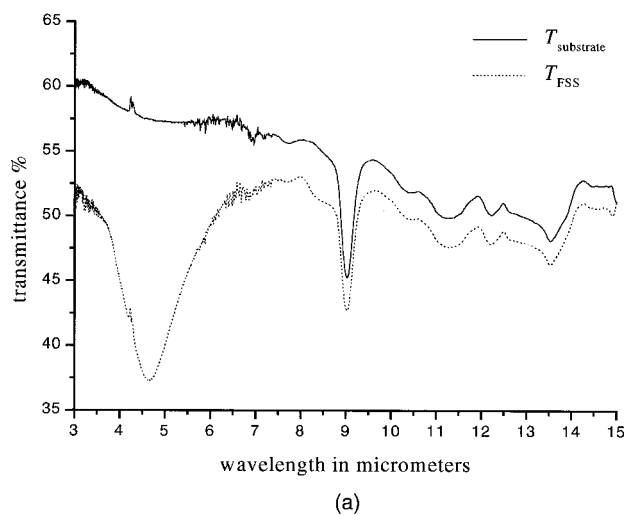


Fig. 1. Spectral (a) transmittance and (b) reflectance of the FSS and of the substrate alone for array type (air-Si, coupled, 0.8).

the transmission and reflection of the IR FSS will differ from that of the substrate even for wavelengths away from the main resonance. The presence of Al structures on top of the substrate lowers the transmittance and increases the reflectance by a few percent across the entire band, compared with the Si substrate alone. It can also be seen that the specific spectral features of the substrate (especially near $9\ \mu\text{m}$) tend to obscure the resonant response of the dipole arrays. The absorption at $9\ \mu\text{m}$ is caused by a Si-O lattice vibration arising from oxygen occluded during the crystal growth or from oxidation of the substrate surface in contact with the atmosphere.¹⁷

As shown in Fig. 2, we emphasize the resonant nature of the spectral features by plotting a spectral transmittance and reflectance of each FSS normalized to those of the substrate:

$$\hat{T} = T_{\text{FSS}}/T_{\text{substrate}}, \quad (1)$$

$$\hat{R} = R_{\text{FSS}}/R_{\text{substrate}}. \quad (2)$$

4. Interelement Spacing

One goal of our study was to investigate whether there exists, for our choice of materials and geometry, a resonance mode for the FSS that is feed coupled.

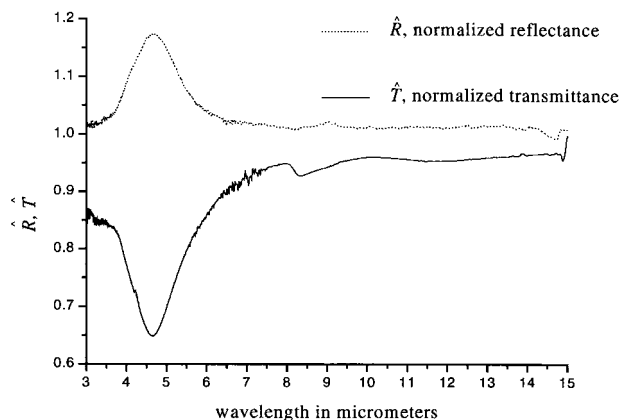
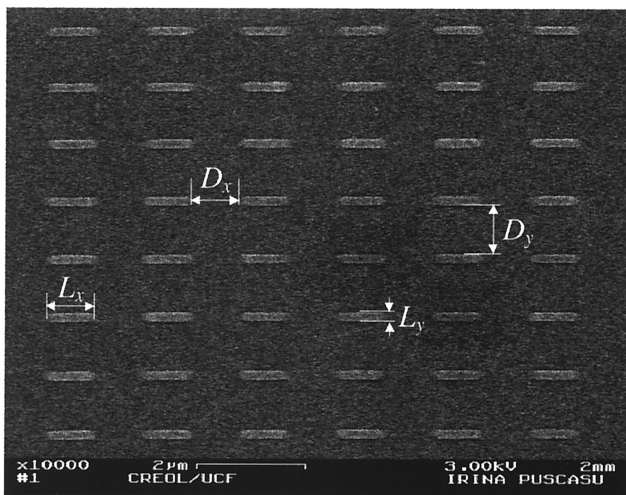
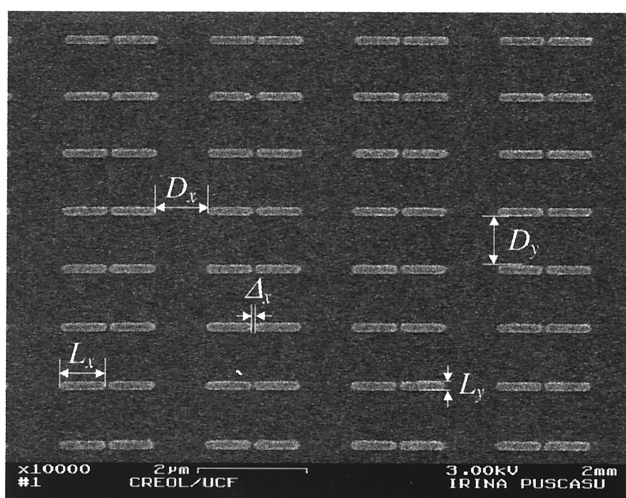


Fig. 2. Spectral transmittance and reflectance of the FSS normalized to the transmittance and reflectance, respectively, of the bare substrate.



(a)



(b)

Fig. 3. Scanning electron micrographs of (a) an isolated dipole array and (b) a coupled dipole array.

Specifically, we fabricated two types of array configuration, as seen in Fig. 3. One FSS, “isolated,” is composed of individual patch elements, of arm length L_x , with an equal edge-to-edge spacing ($D_x = D_y$) in both directions. The other FSS, “coupled,” is composed of the same size patches but arranged with a very small interelement spacing ($\Delta_x = 0.1 \mu\text{m}$) in the x direction for adjacent patches. The resulting pairs of patches are spaced by the same edge-to-edge spacing as in the previous FSS. These structures were fabricated directly on the Si substrate for arm lengths $L_x = 0.8 \mu\text{m}$ and $1.6 \mu\text{m}$. In Fig. 4 we compare the normalized spectral transmittance of these FSS’s. The locations of the resonances of the isolated and coupled FSS’s are virtually identical and are consistent with the dependence on arm length and refractive indices presented in Section 5. The patches for the coupled FSS resonated nearly as independent

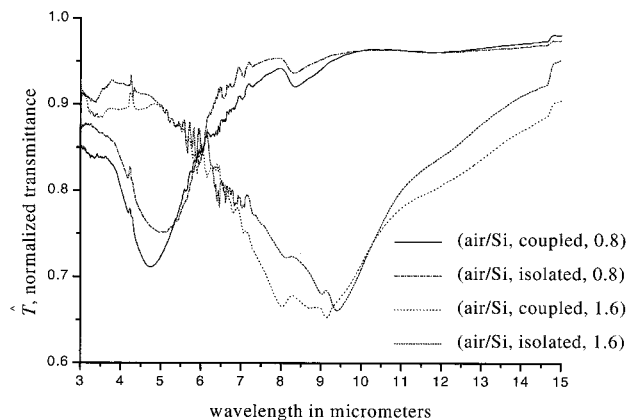


Fig. 4. Comparison between isolated and coupled dipole array transmittance response.

dipoles of length L_x . There was no significant resonance noted for which the two closely spaced patches behaved as two arms of a dipole antenna, coupled through the sheet resistance in the enhanced-field feed region between the arms.

The only difference noted in the normalized transmittance was a slight shift of the resonance toward shorter wavelengths for the coupled FSS, and a slight broadening of the resonance. The wavelength shifts are consistent with the fact that the resonance of a dipole array is reached when the impedance of the elements is purely resistive. In this case, $X_{\text{self}}(\lambda) + X_{\text{mut}}(\lambda) = 0$, where $X_{\text{self}}(\lambda)$ and $X_{\text{mut}}(\lambda)$ represent the self-reactance and the mutual reactance, respectively. Near the resonance wavelength, $X_{\text{self}}(\lambda)$ decreases as the wavelength increases and $X_{\text{mut}}(\lambda)$ is negative.¹⁸ Thus adding the coupling term given by the mutual reactance to the self-reactance results in a shorter resonance wavelength for the coupled FSS configuration. The slight broadening of the resonance bandwidth for the coupled case, seen in the data in Fig. 4, is consistent with the observation that the half-power bandwidth increases with element density.¹⁹ This density, being inversely proportional to the average distance between the elements, is clearly higher for the coupled FSS configuration.

5. Refractive Index

To investigate the effect of substrate and superstrate refractive indices on the resonance wavelength, we fabricated IR FSS’s with three different cross-sections as seen in Fig. 5. For the case 1 (air-SiO₂) configuration the Al patches of the FSS are deposited on top of the SiO₂ layer. For the case 2 (air-Si) configuration the metal is directly deposited on top of the Si substrate, and in the case 3 (Si-Si) configuration the FSS patches are buried inside a surrounding medium of Si.

The free-space resonance wavelength $\lambda_{0,\text{res}}$ of the FSS is approximately determined by the length of the dipole arm L_x . For an isolated narrow patch in free space, we find theoretically that

$$\lambda_{0,\text{res}} = 2L_x. \quad (3)$$

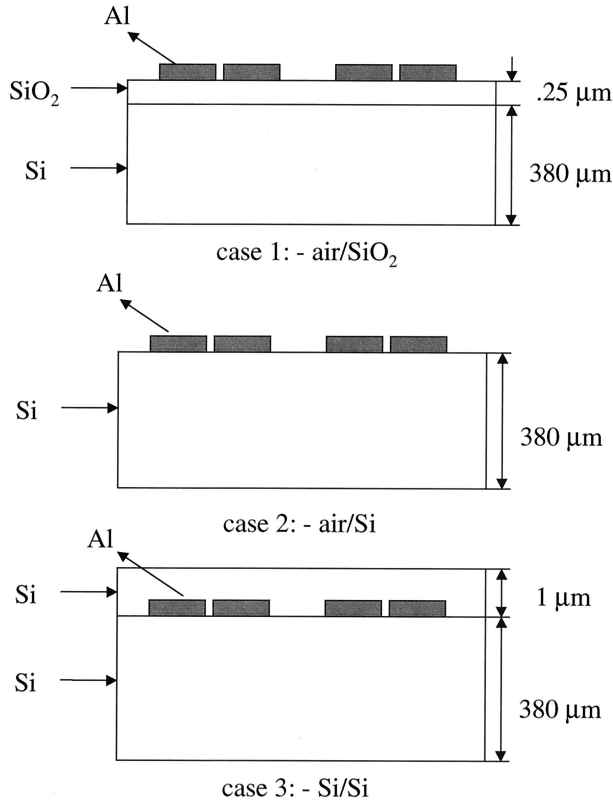


Fig. 5. Configurations of the FSS fabricated: case 1, dipole array supported by a thin layer (2500 Å) of SiO₂ on a Si substrate; case 2, dipole array supported by a Si substrate; case 3, dipole array buried into the Si substrate.

A better approximation of the resonance is obtained when we consider the finite cross-arm width L_y . In this case a single narrow strip exhibits a resonance at approximately¹⁹

$$\lambda_{0,\text{res}} = 2.1L_x(1 + L_y/2L_x). \quad (4)$$

Equations (3) and (4) above apply for patches in free space. For patches with a refractive index n_1 above and n_2 below, the actual resonance wavelength is modified by the effective index n_{eff} of the two-layer medium

$$\lambda_{\text{res}} = \lambda_{0,\text{res}}n_{\text{eff}}, \quad (5)$$

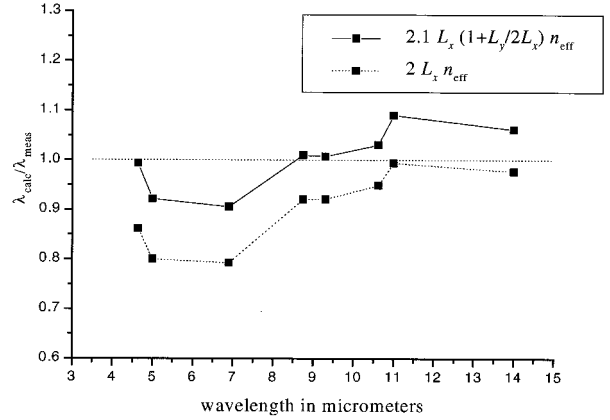


Fig. 6. Ratio of the calculated wavelength of resonance with respect to the measured wavelength of resonance with Eq. (3) and Eq. (4), respectively, as a function of measured wavelength of resonance.

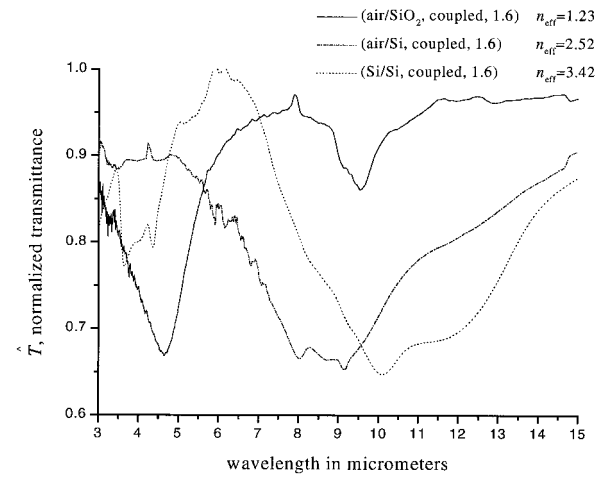


Fig. 7. Spectral transmittance of a dipole array on a SiO₂ layer [type (air-SiO₂), coupled, 1.6], on a Si substrate [type (air-Si, coupled, 1.6)], and buried in Si [type (Si-Si, coupled, 1.6)].

where n_{eff} is given by

$$n_{\text{eff}} = [(n_1^2 + n_2^2)/2]^{1/2}. \quad (6)$$

We observe that Eq. (6) is symmetric in n_1 and n_2 , which is proved by the fact that the wavelength of

Table 2. Theoretical and Experimental Values of the Resonant Wavelength for the Arrays Fabricated

Name ^a	n_{eff}	λ_{res} measured (μm)	$\lambda_{\text{res}} = 2.1L_x(1 + L_y/2L_x)n_{\text{eff}}$ (μm)	$\lambda_{\text{res}} = 2.1L_x n_{\text{eff}}$ (μm)
(air-SiO ₂ , coupled, 1.6)	1.23	4.63	4.31	3.94
(air-Si, coupled, 0.8)	2.52	4.64	4.61	4.00
(air-Si, coupled, 1.6)	2.52	8.75	8.84	8.06
(air-Si, coupled, 2)	2.52	10.62	10.95	10.08
(air-Si, isolated, 0.8)	2.52	5.00	4.61	4.00
(air-Si, isolated, 1.7)	2.52	9.30	9.37	8.57
(Si-Si, coupled, 0.8)	3.42	6.90	6.25	5.47
(Si-Si, coupled, 1.6)	3.42	11.0	12.0	10.94
(Si-Si, coupled, 2)	3.42	14.0	14.87	13.68

^aSubstrate configuration, array configuration, dipole length L_x (μm).

resonance in the transmission spectra is experimentally seen to be independent of the direction of the incident radiation. This is perhaps surprising in view of Brewitt-Taylor's results²⁰ that compare the amplitude of antenna patterns for dipoles on a dielectric half-space and find a factor of $\epsilon^{3/2}$ for the proportionality, equivalent to ≈ 40 for an air-Si interface. His theory, though, assumed wavelengths larger than 30 μm and was applied for loaded antennas, which is different from our case.

Using an approximate index of 3.42 for Si and 1.37 for SiO_2 (Ref. 21) at the particular resonant wavelengths, in Eqs. (3) and (4), we obtained the values for the wavelength of resonance in Table 2. We observe that Eq. (4) gives a better approximation of the wavelength of resonance for wavelengths smaller than 11 μm (Fig. 6).

The presence of the substrate in the vicinity of the array plays an important role in the spectral response of the array. In Fig. 7 we present transmission data for the same array in three different substrate configurations: on a SiO_2 layer [type (air- SiO_2 , coupled, 1.6)], on a Si substrate [type (air-Si, coupled, 1.6)], and buried in Si [type (Si-Si, coupled, 1.6)]. As the effective index of refraction increases, the wavelength of resonance (the minimum in the transmission data) shifts toward longer values in agreement with Eq. (4).

6. Conclusions

Frequency-selective surfaces have been fabricated by *e*-beam lithography in several configurations. Measurements of spectral reflection and transmission have demonstrated resonant behavior at different wavelengths in the 4–12- μm range. The presence of the superstrate and substrate media shifts the resonance wavelength of the FSS compared with the value calculated in air. The scaling factor is the effective index, calculated as the square root of the average dielectric permittivity. Higher effective indices shift the resonance toward longer wavelengths. The resonance wavelength is independent of the illumination direction, as required by the fact that the effective index is symmetric in the superstrate and substrate indices. The primary resonance mechanism of the FSS's is the resonance of the individual metallic patches. There is no discernible resonance arising from a feed-coupled configuration, even for a 0.1- μm interelement spacing. For the FSS's with these closely spaced elements, we did however observe a shift of the resonance toward shorter wavelengths and a slight broadening of the resonance behavior.

References

1. R. Ulrich, "Far-infrared properties of metallic mesh and its complementary structure," *Infrared Phys.* **7**, 37–55 (1967).
2. J. G. Gallagher and D. J. Brammer, "Scattering from an infinite array of periodic broken wires buried in a dielectric sheet," *Radio Sci.* **20**, 50–62 (1985).
3. R. Mittra, C. Chan, and T. Cwik, "Techniques for analyzing frequency selective surfaces—a review," *IEEE Proc.* **76**, 1593–1615 (1988).
4. E. L. Pelton and B. A. Munk, "Scattering from periodic arrays of crossed dipoles," *IEEE Trans. Antennas Propag.* **AP-27**, 323–330 (1979).
5. S. M. A. Hamdy and E. A. Parker, "Influence of lattice geometry on transmission of electromagnetic waves through arrays of crossed dipoles," *IEEE Proc. Part H* **129**, 7–10 (1982).
6. C. H. Tsao and R. Mittra, "Spectral domain analysis of frequency selective surfaces comprised of periodic arrays of crossed dipoles and Jerusalem crosses," *IEEE Trans. Antennas Propag.* **AP-32**, 478–486 (1984).
7. R. J. Langley and A. J. Drinkwater, "Improved empirical model for the Jerusalem cross," *IEEE Proc. Part H* **129**, 1–6 (1982).
8. J. C. Vardaxoglou and E. Parker, "Performance of two tripole arrays as frequency selective surfaces," *Electron. Lett.* **19**, 709–710 (1983).
9. S. M. Hamdy and E. A. Parker, "Current distribution on elements of a square loop frequency selective surface," *Electron. Lett.* **18**, 624–626 (1982).
10. K. J. Kogler and R. G. Pastor, "Infrared filters fabricated from submicron loop antenna arrays," *Appl. Opt.* **27**, 18–19 (1988).
11. T. Timusk and P. L. Richards, "Near millimeter wave bandpass filters," *Appl. Opt.* **20**, 1355–1358 (1981).
12. S. E. Whitcomb and J. Keene, "Low-pass interference filters for submillimeter astronomy," *Appl. Opt.* **19**, 197–198 (1980).
13. V. P. Tomaselli, D. C. Edewaard, P. Gillian, and K. D. Moller, "Far-infrared bandpass filters from crossed-shaped grids," *Appl. Opt.* **20**, 1361–1366 (1981).
14. C. M. Rhoades, E. K. Damon, and B. A. Munk, "Mid-infrared filters using conducting elements," *Appl. Opt.* **21**, 2814–2816 (1982).
15. D. M. Byrne, A. J. Brouns, F. C. Case, R. C. Tiberio, B. L. Whitehead, and E. D. Wolf, "Infrared mesh filters fabricated by electron-beam lithography," *J. Vac. Sci. Technol. B* **3**, 268–271 (1985).
16. M. D. Morgan, W. E. Horne, V. Sundaram, J. C. Wolfe, S. V. Pendharkar, and R. Tiberio, "Application of optical filters fabricated by masked ion beam lithography," *J. Vac. Sci. Technol. B* **14**, 3903–3906 (1996).
17. T. Sato, "Spectral emissivity of silicon," *Jpn. J. Appl. Phys.* **6**, 339–347 (1967).
18. J. D. Kraus, *Antennas*, 2nd ed. (McGraw-Hill, New York, 1988).
19. S. T. Chase and R. D. Joseph, "Resonant array bandpass filters for the far infrared," *Appl. Opt.* **22**, 1775–1779 (1983).
20. C. R. Brewitt-Taylor, D. J. Gunton, and H. D. Rees, "Planar antennas on a dielectric surface," *Electron. Lett.* **17**, 729–731 (1981).
21. E. D. Palik, *Handbook of Optical Constants of Solids* (Academic, New York, 1985)